IEEE Access
Multidisciplinary ⋮ Rapid Review ⋮ Open Access Journal

Received 17 April 2023, accepted 26 April 2023, date of publication 1 May 2023, date of current version 5 May 2023.

Digital Object Identifier 10.1109/ACCESS.2023.3271717

RESEARCH ARTICLE

Autonomous Berthing of Unmanned Surface Vehicles Based on Improved Dubins-RRT Algorithm and Non-Singular Terminal Sliding Mode Control

FEIFEI SONG[1], XIAOFEI YANG[2], (Member, IEEE), AND ZHENGRONG XIANG[3], (Member, IEEE)

[1]Kangda College of Nanjing Medical University, Lianyungang 222006, China
[2]College of Automation, Jiangsu University of Science and Technology, Zhenjiang 212000, China
[3]School of Automation, Nanjing University of Science and Technology, Nanjing 210094, China

Corresponding author: Xiaofei Yang (yxfei_0809@just.edu.cn)

This work was supported in part by the Science and Technology Innovation Group Program of the Kangda College of Nanjing Medical University, under Grant KD2022KYCXTD003; in part by the Brand Specialty Construction Project of the Kangda College of Nanjing Medical University, under Grant JX206000302; and in part by the National Natural Science Foundation of China under Grant 62203191.

ABSTRACT Autonomous berthing is the last step to achieving the autonomous operation of unmanned surface vehicles (USVs). Due to the significant disturbance of wind, waves, and currents and the uncertainties of the model, it is difficult to realize autonomous berthing. For the case of obstacles and dynamics of USVs, it is transformed into three steps including path planning, path tracking, and motion control of USVs in the paper. A new advanced Dubins-RRT algorithm is proposed for path planning, which improves the capacity of obstacle avoidance and path smoothness level. A virtual target guidance method is used to guide and track the planned path. In addition, a finite-time disturbance observer and a non-singular terminal sliding mode controller are designed to control the autonomous USVs. Observing and estimating the uncertainty terms in the model can ensure the convergence of the tracking error in a finite time. Finally, the feasibility of the designed method is verified through simulation and experimentation.

INDEX TERMS Autonomous berthing, USVs, path planning, virtual target guidance, terminal sliding mode control.

I. INTRODUCTION

Autonomous USVs are surface mission platforms with capabilities of environmental sensing, path planning, navigation, and control [1], [2]. Compared to traditional marine equipment, they are smaller in size, more maneuverable, and more intelligent. They can perform various dangerous tasks without casualties and are widely used in military and civilian fields [3], [4], with typical equipment shown in Fig. 1. For autonomous USVs, autonomous berthing is the last step. Due to the low speed in shallow water, disturbances from wind, waves, and currents, and underactuated, it is also complex and challenging. Therefore, many researches have been carried out on the autonomous berthing of USVs.

FIGURE 1. Typical unmanned surface vehicles.

There are three types of berthing methods for USVs: stern-first berthing, bow-first berthing, and lateral approach,

The associate editor coordinating the review of this manuscript and approving it for publication was Shihong Ding.

as shown in Fig. 2. Due to not being consistent with the dynamics of USVs, stern-first berthing is rare. The lateral approach is common, such as an adaptive model reference controller for the lateral approach with uncertain dynamic characteristics is designed and good results are obtained [5]. Reference [6] has addressed the model uncertainty problem and designed a dynamic surface control (DSC) based on backstepping and Lyapunov direct methods during berthing, which is effective in the lateral approach. Reference [7] has combined the artificial potential field method to achieve a berth in an environment with obstacles for the lateral approach. In addition, direct bow-first berthing is also a common berthing method with the advantage of no special requirements for the environment.

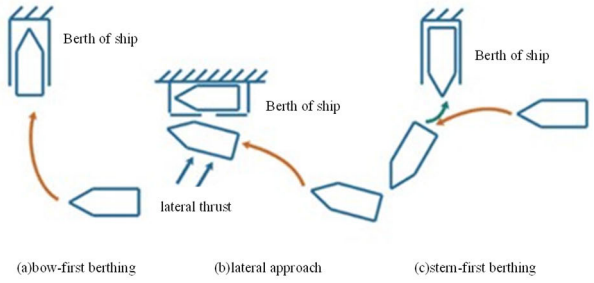

FIGURE 2. Schematic diagram of docking schemes.

In recent years, there have been many studies on the motion control of USVs, but relatively few on autonomous berthing. It can be decomposed into three steps: path planning, guidance law design, and motion control. The methods of path planning can be divided into four categories: graph search, virtual potential field, random sampling, and intelligent algorithms. Graph search algorithms mainly rely on geometric shapes, including Dijkstra's algorithm and A* algorithm. In Dijkstra's algorithm, a greedy approach is used to solve the shortest path problem from one node to another. It has low efficiency and is often used in combination with other algorithms. The A* algorithm is a heuristic algorithm that establishes heuristic search rules to measure the distance from the target, prioritizing the search direction towards the target, and improving the search efficiency [8]. The concept of potential fields is drawn in the virtual potential field method, a virtual potential field is constructed in the map, and a smoother path can be generated. The new attractive and repulsive potential field functions are designed and a new process of dynamic collision avoidance is constructed to ensure safe collision avoidance of USVs [9]. The rapidly exploring random tree (RRT) method is a random sampling algorithm, which tends to search for unexplored areas of space. A space-filling tree is randomly constructed to search the nonconvex high-dimensional space to improve efficiency. It is fast and scalable, and widely used in path planning in dynamic environments [10]. The planned path is consistent with the dynamics of USVs. However, the search of the RRT algorithm is not directional, and the path is not optimal. Despite the drawbacks, various improvements have been made. Focusing on narrow channels and unevenly distributed obstacles, a variable-step RRT* algorithm is proposed that changes the fixed step to a variable step, and proved that it is better than the RRT and RRT* algorithms [11]. A quick-RRT* method is proposed by extending the set of possible parent nodes in [12], which obtains a lower-cost path than the RRT* algorithm. Potential Function Based-RRT* (P-RRT*) is combined with Q-RRT* to obtain the PQ-RRT* algorithm, which can quickly converge to an optimal solution, and the effectiveness of the algorithm is validated through simulation [13]. Recently, the reinforcement learning approach has been utilized for the path planning of USVs. For example, a Q-learning-based path planning algorithm has been designed for smart ships. The effectiveness of the method has been demonstrated and compared with the traditional path planning methods [14]. In [15] the deep deterministic policy gradient (DDPG) algorithm is utilized for path planning of the unmanned ship. An optimized DQN algorithm is proposed with an improved reward function, and achieves better planning results [16]. A global path planning algorithm based on DDQN is proposed for amphibious USV. The paths generated by the proposed method have better performance by comparing with DQN, A*, and RRT algorithms [17].

In order to follow a path, appropriate guidance laws are needed. Common guidance laws include the line-of-sight (LOS) [18] and virtual target methods [19]. Based on the basic LOS algorithm, the predictor LOS (PLOS) [20], integral LOS (ILOS) [21], adaptive LOS (ALOS) [22], and other algorithms are proposed. The virtual target method is also commonly used. The LOS algorithm and virtual target method are combined to convert the tracking problem into a guidance problem with angle constraints [23]. Cascade control is adopted to conquer the tracking and control problem of USVs. And a tracking error dynamics model is established to generate a reference trajectory for a virtual leader to achieve the guidance [24]. In addition, effective control of USVs is required to generate the desired signal for tracking. To address the problem of unknown disturbances, various control algorithms have been proposed to design corresponding controllers, such as backstepping control [25], adaptive control [26], neural network control [27], sliding mode control [28], etc. In [29] the unknown functional bounds of uncertainties in the system are modeled by fuzzy logic systems, and an adaptive fuzzy fixed-time high-order sliding mode controller is designed to fulfill the pre-set constraint condition. It also has the advantages of good transient response and strong robustness by the sliding mode control [30]. To achieve finite time convergence, nonsingular terminal sliding mode control (TSMC) [31] and nonsingular fast TSMC [32] are adopted in the design of controllers for trajectory tracking. The super-twisting method is a better sliding mode method to reduce chatting for USV control [33]. The problem of steering gear wear is also addressed, an active disturbance rejection control (ADRC) method based

on linear sliding mode is proposed and its effectiveness is verified through simulation [34]. A globally asymptotically stable tracking controller for USVs is proposed based on the nonlinear backstepping sliding mode method and Lyapunov stability theory, with characteristics of insufficient power and asymmetry, and its effectiveness is verified through simulation [35]. To address the effects of the sideslip angle, a finite-time predictor LOS-based integral sliding mode adaptive neural (FPISAN) scheme is proposed, and simulation results show good control performance [36].

Inspired by previous research, autonomous berthing of the USVs is converted into a navigation, guidance, and control problem of the bow-first berthing mode in the paper. Due to the obstacles and inertia, the path planned should be with obstacle avoidance and smoothness. Therefore, the Dubins method is integrated into the RRT algorithm to obtain a smoother path. A guidance law based on the virtual target method is designed and a controller based on global non-singular terminal sliding mode (NTSM) is also designed. The main contributions of the paper are as follows,

1) To make the path smoother, especially poses of the starting and ending, a new improved Dubins-RRT algorithm is proposed to plan the berthing path. The straight-line extension random tree of the RRT algorithm is replaced by the Dubins path. It can obtain a smoother path that also satisfies the dynamics of USVs.

2) For the control of the USVs, a global NTSM controller is designed, which is suitable for nonlinear dynamic systems with parameter uncertainty and external disturbances. In the controller, the non-singular terminal sliding mode surface is designed to overcome the singularity problem of the common terminal sliding mode controller, and any initial state can converge to the sliding mode surface in a finite time.

3) Simulation and field experiments are carried out to validate its effectiveness.

The remainder of the paper is organized as follows. The kinematic and dynamic model of the USVs and the control objective is introduced in Section II. A new path planning method of Dubins-RRT is proposed under the multi-obstacle environment in Section III-A. In Section III-B, the virtual target guidance method is proposed to guide the USVs. The finite-time disturbance observer and the non-singular terminal sliding mode controller are designed in Section III-B and Section 3.3, respectively. Section IV provides a simulation and experimental results to validate our method. Finally, conclusions are summarized in Section V.

II. PRELIMINARY KNOWLEDGE AND PROBLEM FORMATION

A. COORDINATE SYSTEM OF USVs

The body-fixed frame and earth-fixed inertial frame are two common coordinate systems for the USVs. They can be used to describe the motion and attitude of the USVs, as shown in Fig.3. The earth-fixed inertial frame is used to describe the positional state of the USVs, and the body-fixed frame is used to describe the linear velocity and angular rate of the USVs. The center of gravity is consistent with the origin of the body-fixed frame, represents the longitudinal axis from the stern to the bow, represents the lateral axis pointing to the starboard, and represents the vertical axis pointing to the center of the earth. Similarly, is the north, is the east, and is perpendicular to the stationary horizontal plane and points to the center of the earth. The specific meaning of each symbol is given in Table 1.

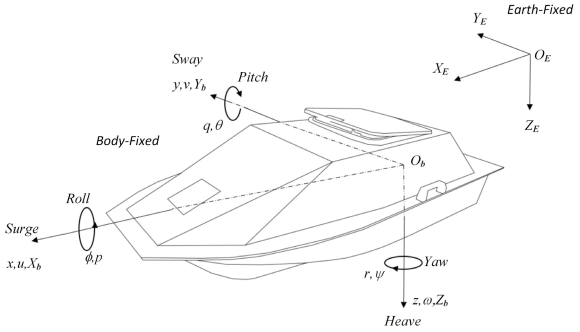

FIGURE 3. Coordinate system of the USVs.

TABLE 1. Six-DOF motion symbols of the USVs.

motion state	velocity and angular rate	Position and Euler angle
Surge	u	x
Sway	v	y
Heave	w	z
Roll	p	ϕ
Pitch	q	θ
Yaw	r	ψ

B. KINEMATICS AND DYNAMICS MODEL OF THE USVs

During autonomous berthing, it has a relatively trial impact in the roll, pitch, and heave. To facilitate the design of the controller, the following assumptions are given,

1) Only surge, sway, and yaw are considered, thus, $z = 0, \phi = 0, \theta = 0, w = 0, p = 0\sqrt{b^2 - 4ac}$ and $q = 0$.

2) The mass of the USVs is uniformly distributed, and is symmetrical about the x and$z$ axis, thus, $I_{xy} = I_{YX} = 0$.

3) The centers of gravity and buoyancy are both on the $O_B z_B$.

The kinematics of the USVs is represented as follows [37],

$$\begin{cases} \dot{x} = u\cos\psi - v\sin\psi, \\ \dot{y} = u\sin\psi + v\cos\psi, \\ \dot{\psi} = r, \end{cases} \tag{1}$$

where, (x, y) is the position, ψ is the heading angle; u and v denote the linear velocities of surge and sway, and r is the angular rate of yaw, respectively.

To facilitate the observer and controller design, the uncertainties are combined and the motion model of the USVs are written in the following,

$$\begin{cases} \dot{\eta} = J(\eta)\upsilon \\ M_{RB}\dot{\upsilon} + C_{RB}(\upsilon)\upsilon = \tau + \tau_E \end{cases}$$
$$J(\eta) = \begin{pmatrix} \cos\psi & -\sin\psi & 0 \\ \sin\psi & \cos\psi & 0 \\ 0 & 0 & 1 \end{pmatrix},$$
$$M_{RB} = \begin{pmatrix} m & 0 & 0 \\ 0 & m & 0 \\ 0 & 0 & I_z \end{pmatrix},$$
$$C_{RB} = \begin{pmatrix} 0 & 0 & -mv \\ 0 & 0 & mu \\ mv & -mu & 0 \end{pmatrix} \quad (2)$$

External disturbances $\tau_E = (\tau_{uE}, \tau_{vE}, \tau_{rE})^T$ are written as,

$$\tau_E = -M_A\dot{\upsilon} - C_A(\upsilon)\upsilon - D(\upsilon)\upsilon - g(\eta)$$

where M_A is the added mass matrix; $C_A(\upsilon)$ is Coriolis and centripetal force matrix; $D(\upsilon)$ is the damping matrix; and $g(\eta)$ is the restoring force and moment vector.

C. PROBLEM STATEMENT

In the paper, the autonomous berthing of USVs is transformed into a navigation, guidance, and control problem to track a planned path, and can be solved by three steps, as shown in Fig. 4.

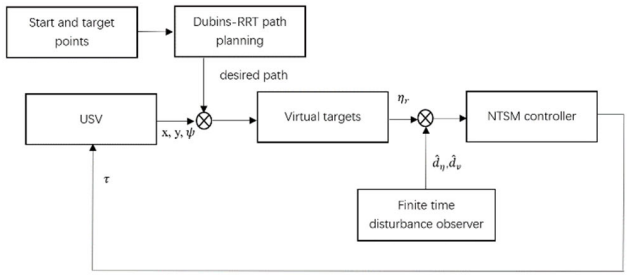

FIGURE 4. Flow chart of autonomous berthing of the USV.

The berthing path should be planned first. Considering the characteristics of underactuation, it needs certain smoothness. In addition, obstacle avoidance capability is also requirement. Due to the large inertia, it is difficult to make rapid turns and translations. To obtain smooth path and advance obstacle avoidance capability, the path should meet the requirements of the starting and ending positions of the USVs. So, Dubins path and RRT algorithm are introduced and improved to obtain a smooth path and meet the characteristics of the USVs. To track the planned path, the virtual leader method is also used to guide the USVs. The expected pose of the virtual leader is $\eta_R = [x_R, y_R, \psi_R]$, and the tracking error $\eta_e = \eta - \eta_R$, $\eta_e = [x_e, y_e, \psi_e]$. To track the planned path, control laws $\tau_u$andτ_r are designed to make η_e tend to 0 in a finite time.

III. AUTONOMOUS BERTHING PATH PLANNING AND CONTROL LAW DESIGN

A. PATH PLAN ALGORITHM BASED ON DUBINS AND RRT

Considering the dynamics of underactuated USVs and the requirements for path planning, a new improved Dubins-RRT path planning algorithm is proposed. The straight-line extension random tree of the RRT algorithm is replaced by the Dubins path. For any starting and ending poses, at least four different curves can be obtained, and it is impossible to determine the unique path between the two points. The shortest Dubins path is defined as the unique path during the growth of the random tree. To determine its length, each Dubins curve path should be calculated, it is time-consuming and nonfeasible. So, it has been improved in the paper. According to the definition of Dubins path, CSC, CCC, and their sub-paths are continuous differentiable curves, and there must be an optimal path in each group. To convert any point $(x, y, \varphi) \in R^3$ into a corresponding phase point, three operators are defined: L_v (left turn), R_v (right turn), and S_v (straight line). The definitions of these operators are as follows,

$$L_v(x, y, \phi) = \begin{pmatrix} x + \sin(\phi + l) - \sin\phi \\ y - \cos(\phi + l) + \cos\phi \\ \phi + l \end{pmatrix}$$
$$R_v(x, y, \phi) = \begin{pmatrix} x - \sin(\phi - l) + \sin\phi \\ y + \cos(\phi - l) - \cos\phi \\ \phi - l \end{pmatrix}$$
$$S_v(x, y, \phi) = \begin{pmatrix} x + l\cos\phi \\ y + l\sin\phi \\ \phi \end{pmatrix} \quad (3)$$

Among them, l is the length of arc or segment in the Dubins. After the conversion, any curve in the Dubins path set D = {RSR, RSL, RLR, LSL, LSR, LRL } can be expressed through the corresponding operator. Given the starting pose is $(0, 0, \varphi_S)$, the ending pose is $(d, 0, \varphi_S)$, and the Euclidean distance between them is D_E. Let $d = D_E/R$, R is the minimum turning radius of the USVs. If the curve is LRL and the starting pose is $(0, 0, \varphi_S)$, and the lengths of the three segments are a, b, c, respectively, then the endpoint must be $(d, 0, \varphi_S)$ and $L_c(R_b(L_a(0, 0, \varphi_S))) = (d, 0, \varphi_S)$. The total length L of the curve is as shown in (4),

$$L = a + b + c \quad (4)$$

Similarly, the calculation of curve length can be obtained based on the type in set D, which can be found in reference [38]. It can be used to quickly and easily obtain the shortest path. In the RRT algorithm, the growth of the tree depends on the randomly generated point $Q_{rand} = (x_{rand}, y_{rand})$, which lacks pose information. So, the pose information should be added to satisfy the conditions for generating Dubins paths. Sampling point Q is obtained from random sampling. If the sampling point is within the obstacle, then sampling process needs to be rerun. The pseudocode of the new improved Dubins-RRT is shown in Table 2.

TABLE 2. Pseudocode of the Dubins-RRT algorithm.

Input: Map, $Q_{init} = (x_{init}, y_{init}, \psi_{init})$, $Q_{goal} = (x_{goal}, y_{goal}, \psi_{goal})$
Output: Path
Step 1: Process the map and convert it into a grayscale map
Step 2: Path planning with Dubins-RRT
Let the random tree be T and there is T. $init(Q_{init})$
for k=1 to K
Take a random pose point on the map Q_{rand}
Find the pose point $Q_{nearest}$ nearest to Q_{rand} in T
If(There is a Dubins curve between $Q_{nearest}$ and Q_{rand}):
List all possible Dubins curve types to find the shortest one
if (Q_{rand} does not collide with obstacles)
Add Q_{rand} as a new node to tree T
else abandon Q_{rand}, give up this growth, jump out of the loop
end
else
Abandon, Q_{rand}, give up this growth, continue the cycle
end
If(The distance from Q_{new} to the end point Q_{goal} is less than ε)
The target point has been found, the loop exits, and the path planning is completed.
Else
Continue the loop
end
end

B. GUIDANCE AND CONTROL LAW DESIGN

1) VIRTUAL TARGET GUIDANCE

To track the planned path, a virtual leader can be set, and the USVs can be guided to track the virtual leader. Assume that:

1) The hydrodynamic coefficients and dynamics of the virtual leader are consistent with the USVs.

2) The path expected can be described as a sufficiently smooth time function generated by the motion of the virtual leader with the time parameter t.

3) The center of the virtual leader coincides with the reference point of the expected path, and the speed of the virtual leader is greater than zero, i.e., the virtual leader cannot move backward.

In the inertial coordinate system, the center of mass of the leader can be expressed as $m_R = [x_R, y_R]^T$, and the virtual leader is along the desired path, as shown in Fig. 5.

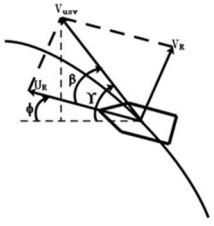

FIGURE 5. Guidance based on virtual target.

Assume the speed of the virtual leader is v_D, and $v_D = \| v_D \| = \| \dot{m}_R \| = \sqrt{\dot{x}_R + \dot{y}_R}$. Correspondingly, the first-order derivative is $\dot{v}_D$, and the second-order derivative is $\ddot{v}_D$. The lateral velocity of the virtual leader is given by $v_R = \pm\sqrt{v_D^2 - u_R^2}$, where u_R is the longitudinal velocity, and the sign of $\pm$ is the direction. According to the planned path, the virtual leader may turn left or right. As assumption 3, it can only move forward, which means $u_R > 0$. The sign of the lateral velocity v_r depends only on the yaw rate r_R. When $r_R > 0$, v_R is positive, otherwise, v_R is negative. When $u_R = v_D$, the lateral velocity, lateral acceleration, and their time derivatives are all zero. In the process of autonomous berthing, the longitudinal velocity u_R is a constant. Consequently, the longitudinal acceleration $\dot{u}_R$ and the second-order derivative of the longitudinal velocity $\ddot{u}_R$ are both zero.

From Fig. 5, it can be seen that the expected yaw angle $\psi_R = \gamma - \beta$, sideslip angle $\beta = \arctan\frac{v_R}{u_R}$ and heading angle $\gamma = \arctan\frac{\dot{y}_R}{\dot{x}_R}$. It can be deduced that the yaw rate

$$r_R = \omega - \frac{\dot{v}_R u_R - \dot{u}_R v_R}{v_D^2},$$

and $\dot{r}_R = \dot{\omega} - \frac{\ddot{v}_R u_R - \dot{u}_R v_R}{v_D^2} + 2\frac{\dot{v}_R u_R - \dot{u}_R v_R}{v_D^3}\dot{v}_D$, where angular velocity of heading angle $\omega = \frac{\dot{x}_R \ddot{y}_R - \ddot{x}_R \dot{y}_R}{v_D^2}$, $\dot{\omega} = \frac{\dot{x}_R y_R - x_R \dot{y}_R}{v_D^2} - 2\frac{\omega \dot{v}_D}{v_D}$.

To obtain the relationship between the actual state and the desired path, the tracking error equation is

$$\eta_e = \eta - \eta_R, \quad \eta_e = [x_e, y_e, \psi_e],$$

The desired position and pose of the virtual leader is $\eta_R = [x_R, y_R, \psi_R]$.

$$\dot{\eta}_e = \dot{\eta} - \dot{\eta}_R \tag{5}$$

Expand (5) and simplify it,

$$\dot{\eta}_e = J(\eta)\upsilon_e - (J(\eta) - J(\eta_R))\upsilon_R \tag{6}$$

where, $\upsilon_R = [u_R, v_R, r_R]$ is the expected speed of the virtual leader, and $\upsilon_e = [u_e, v_e, r_e]$ is velocity tracking error. Since there are uncertainties in the dynamics and kinematics models of the USVs, and can be given as follows,

$$\begin{aligned} d_\eta &= (J(\eta) - J(\eta_R))\upsilon_R \\ d_\eta &= [d_{\eta 1}, d_{\eta 2}, 0] \end{aligned} \tag{7}$$

Then (6) can be rewritten as follows,

$$\dot{\eta}_e = J(\eta)\upsilon_e + d_\eta \tag{8}$$

Combined with (2), the speed of the virtual leader can be obtained,

$$\dot{\upsilon}_e = \dot{\upsilon} - \dot{\upsilon}_R = M_{RB}^{-1}(-C_{RB}(\upsilon)\upsilon + \tau_H + \tau) - \dot{\upsilon}_R \tag{9}$$

Thus, the tracking error equation is obtained,

$$\begin{cases} \dot{\eta}_e = J(\eta)\upsilon_e + d_\eta \\ \dot{\upsilon}_e = \dot{\upsilon} - \dot{\upsilon}_R = M_{RB}^{-1}(-C_{RB}(\upsilon)\upsilon + \tau_H + \tau) - \dot{\upsilon}_R \end{cases} \tag{10}$$

2) DESIGN OF FINITE-TIME DISTURBANCE OBSERVER

Due to the influence of wind, waves, currents, and other factors, it is difficult to accurately measure the hydrodynamic coefficients. The uncertain terms are unbenefited to the control performance. The finite-time disturbance observers are used to estimate the disturbances and uncertainties in the system, which make sure that its state variables can be converged in a finite time. So, two finite-time disturbance observers $\hat{d}_\eta$ and $\hat{d}_\upsilon$ are designed. To facilitate the design of the observer, the kinematic equation of the USVs is rewritten as follows,

$$\dot{x}_e = u_e\cos\psi - v_e\sin\psi + d_{\eta 1} \tag{11}$$
$$\dot{y}_e = u_e\sin\psi - v_e\cos\psi + d_{\eta 2} \tag{12}$$
$$\dot{\psi}_e = r_e \tag{13}$$

System (11) is taken as an example to illustrate the design methodology. It can be rewritten as follows,

$$\dot{x}_e = d_{\eta 1} + f_x \tag{14}$$

where

$$f_x = u_e\cos\psi - v_e\sin\psi \tag{15}$$

and x_e is the state variable, $\psi(t)$ is the input, and these two variables are available in real time. $d_{\eta 1}$ is an uncertain function with $m-1$ derivative, which is unknown disturbance in the system. So, $d_{\eta 1}^{m-1}$ exists, and there is a known Lipschitz constant $L > 0$. At the same time, the input $\psi(t)$ is measurable by Lebesgue.

Assume that u_e is second order derivative, the finite-time disturbance observer is designed

$$\begin{cases} \dot{z}_{x0} = v_{x0} + u_e\cos\psi - v_e\sin\psi \\ v_{x0} = -\lambda_{x0}L_x^{1/4}\left|z_{x0} - x_e\right|^{3/4} sign\left(z_{x0} - x_e\right) + z_{x1} \\ \dot{z}_{x1} = v_{x1} \\ v_{x1} = -\lambda_{x1}L_x^{1/3}\left|z_{x1} - v_{x0}\right|^{2/3} sign\left(z_{x1} - v_{x0}\right) + z_{x2} \\ \dot{z}_{x2} = v_{x2} \\ v_{x2} = -\lambda_{x2}L_x^{1/2}\left|z_{x2} - v_{x1}\right|^{1/2} sign\left(z_{x2} - v_{x1}\right) + z_{x3} \\ \dot{z}_{x3} = -\lambda_{x3}L_x sign\left(z_{x3} - v_2\right) \\ \hat{d}_{\eta 1} = z_{x1}, \hat{\dot{d}}_{\eta 1} = z_{x2} \end{cases} \tag{16}$$

In (16), L_x and $\lambda_{xi}\,(i = 0, 1, \ldots m)$ are the coefficients of the observer. To demonstrate the relationship between z_{xi} and $\hat{d}_{\eta 1}$, propositions are given as following.

Assume that $\psi(t)$ and $f(x_e, \psi)$ can be bounded by Lebesgue measurable noise $\varepsilon > 0$ and $k\varepsilon^{(m-1)/m}$ respectively, where $k > 0$ and is constant. If the parameter λ_{xi} is large enough, then, for normal numbers μ_i and η_i, the following inequalities can be established in a finite time. The establishment of these inequalities depends entirely on the selection of k and parameters

$$\begin{cases} \left|z_{x0} - x_e(t)\right| \le \mu_0\varepsilon \\ \vdots \\ \left|z_{xi} - d_{\eta 1}^{(i-1)}(t)\right| \le \mu_i\varepsilon^{(m-i+1)/(m+1)}, i = 1, \ldots, m, \\ \left|v_i - d_{\eta 1}^{(j)}(t)\right| \le \mu_j\varepsilon^{(m-j)/(m+1)}, j = 0, \ldots, m-1, \end{cases} \tag{17}$$

When there is no input noise, the following exact equation can be established in a limited time

$$\begin{cases} z_{x0} = x_e(t), \\ z_{x1} = f_x(t), \ldots, z_{xi} = v_{i-1} = f_x^{(i-1)}, i = 1, \ldots, m, \end{cases} \tag{18}$$

The proposition is proved. First, define the estimation error

$$\begin{cases} x_{e0} = z_{x0} - x_e(t) \\ x_{e1} = z_{x1} - f_x(t) \\ x_{e2} = z_{x2} - f_x^2 \\ x_{e3} = z_{x3} - f_x^3 \end{cases} \tag{19}$$

From Equations (17), (18) and (19)

$$\begin{cases} \dot{x}_{e0} = -\lambda_0 L^{1/4}\left|x_{e0}\right|^{3/4} sign\left(x_{e0}\right) + x_{e1} \\ \dot{x}_{e1} = -\lambda_1 L^{1/3}\left|x_{e1} - \dot{x}_{e0}\right|^{2/3} sign\left(x_{e1} - \dot{x}_{e0}\right) + x_{e2} \\ \dot{x}_{e2} = -\lambda_2 L^{1/2}\left|x_{e2} - \dot{x}_{e1}\right|^{1/2} sign\left(x_{e2} - \dot{x}_{e1}\right) + x_{e3} \\ \dot{x}_{e3} \in -\lambda_3 L sign\left(x_{e2} - \dot{x}_{e1}\right) + [-L, L] \end{cases} \tag{20}$$

The error of the observer can be stable in a finite time [39]. It can be seen that there is a finite time to make $x_{e3}(t) = 0$.

Similarly, the observer (21) can be designed for (12). According to (16) and (21), the estimation of model uncertainty in the kinematics is realized, and the estimated value is $\hat{d}_\eta = \left(\hat{d}_{\eta 1}, \hat{d}_{\eta 2}, 0\right)^T$. Derivative estimate of uncertainty $\hat{\dot{d}}_\eta = \left(\hat{\dot{d}}_{\eta 1}, \hat{\dot{d}}_{\eta 2}, 0\right)^T$. At the same time, define the estimation error of derivative $\tilde{\dot{d}}_\eta = \dot{d}_\eta - \hat{\dot{d}}_\eta$.

$$\begin{cases} \dot{z}_{y0} = v_{y0} + u_e\sin\psi + v_e\cos\psi \\ v_{y0} = -\lambda_{y0}L_y^{1/4}\left|z_{y0} - y_e\right|^{3/4} sign\left(z_{y0} - y_e\right) + z_{y1} \\ \dot{z}_{y1} = v_{y1} \\ v_{y1} = -\lambda_{y1}L_y^{1/3}\left|z_{y1} - v_{y0}\right|^{2/3} sign\left(z_{y1} - v_{y0}\right) + z_{y2} \\ \dot{z}_{y2} = v_{y2} \\ v_{y2} = -\lambda_{y2}L_y^{1/2}\left|z_{y2} - v_{y1}\right|^{1/2} sign\left(z_{y2} - v_{y1}\right) + z_{y3} \\ \dot{z}_{y3} = -\lambda_{y3}L_y sign\left(z_{y3} - v_{y2}\right) \\ \hat{d}_{\eta 2} = z_{y1}, \hat{\dot{d}}_{\eta 2} = z_{y2} \end{cases} \tag{21}$$

Next, to estimate the model uncertainty in the dynamic equation. First, the dynamics equation of the USVs

is written as follows,

$$\dot{u} = vr + \tau_u + d_{\upsilon 1} \tag{22}$$
$$\dot{v} = -mur + d_{\upsilon 2} \tag{23}$$
$$\dot{r} = \frac{mv}{I_z} r - \frac{mu}{I_z} r + \tau_r + d_{\upsilon 3} \tag{24}$$

where $d_{\upsilon 1} = \tau_{H1}/m, d_{\upsilon 2} = \tau_{H2}/m, d_{\upsilon 3} = \tau_{H3}/I_z$. In this way, the observers of sway and surge motions can be obtained

$$\begin{cases} \dot{z}_{u0} = v_{u0} + vr + \tau_u \\ v_{u0} = -\lambda_{u0} L_u^{1/4} \left| z_{u0} - u \right|^{3/4} sign\left(z_{u0} - u\right) + z_{y1} \\ \dot{z}_{u1} = v_{u1} \\ v_{u1} = -\lambda_{y1} L_y^{1/3} \left| z_{u1} - v_{u0} \right|^{2/3} sign\left(z_{u1} - v_{u0}\right) + z_{u2} \\ \dot{z}_{u3} = -\lambda_{u3} L_u sign\left(z_{u3} - v_{u2}\right) \\ \hat{d}_{\upsilon 1} = z_{u1}, \end{cases} \tag{25}$$

$$\begin{cases} \dot{z}_{v0} = v_{v0} - mur \\ v_{v0} = -\lambda_{y0} L_y^{1/4} \left| z_{y0} - v \right|^{3/4} sign\left(z_{v0} - v\right) + z_{v1} \\ \dot{z}_{v1} = v_{v1} \\ v_{v1} = -\lambda_{v1} L_v^{1/3} \left| z_{v1} - v_{v0} \right|^{2/3} sign\left(z_{v1} - v_{v0}\right) + z_{v2} \\ \dot{z}_{v3} = -\lambda_{v3} L_v sign\left(z_{v3} - v_{v2}\right) \\ \hat{d}_{\upsilon 2} = z_{v1} \end{cases} \tag{26}$$

Similarly, the observer of yaw motion can be written as

$$\begin{cases} \dot{z}_{r0} = v_{r0} \frac{mv}{I_z} r - \frac{mu}{I_z} r + \tau_r \\ v_{r0} = -\lambda_{r0} L_r^{1/3} \left| z_{r0} - r \right|^{2/3} sign\left(z_{r0} - r\right) + z_{r1} \\ \dot{z}_{r1} = v_{r1} \\ v_{r1} = -\lambda_{r1} L_r^{1/2} \left| z_{r1} - v_{r0} \right|^{1/2} sign\left(z_{r1} - v_{r0}\right) + z_{r2} \\ \dot{z}_{r3} = -\lambda_{r3} L_r sign\left(z_{y3} - v_{y2}\right) \\ \hat{d}_{\upsilon 3} = z_{r1} \end{cases} \tag{27}$$

In the way, the estimated model uncertainty value in the dynamics can be obtained $\hat{d}_\upsilon = \left(m\hat{d}_{\upsilon 1}, m\hat{d}_{\upsilon 2}, m\hat{d}_{\upsilon 3}\right)^T$. $\hat{d} = \left(\hat{d}_\eta, \hat{d}_\upsilon\right)$ are the estimated value of the finite-time disturbance observer.

3) DESIGN OF GLOBAL NONSINGULAR SLIDING MODE CONTROLLER

Due to the significant external disturbances, it is difficult to control them effectively in the autonomous berthing. NTSM controller is also devised in the paper. A non-singular terminal sliding mode surface is designed to overcome the singularity problem of terminal sliding mode controller, and any initial state can converge to the sliding mode surface in finite time.

Combined with the finite-time disturbance observer designed in the previous section, a second-order uncertain nonlinear system can be obtained and rewritten in the following,

$$\begin{cases} \dot{\eta}_e = J\left(\eta\right) \upsilon_e + d_\eta \\ \ddot{\eta}_e = \dot{J}\left(\eta\right) \upsilon_e + J\left(\eta\right) \dot{\upsilon}_e + \dot{d}_\eta \end{cases} \tag{28}$$

where $\eta_e = \eta - \eta_R$. J and $\dot{J}$ are smooth nonlinear functions of η. $\dot{d}_\eta$ is the uncertainty in the system and satisfies $\dot{d}_\eta \leq D, D > 0$.

Here, the non-singular sliding surface can be designed as follows,

$$s = \eta_e + K \dot{\eta}_e^{p/q} \tag{29}$$

where, $K = diag\left(k_1, k_2, k_3\right), k_i$ is the constant and $k_i > 0, i = 1, 2, 3$. p and q are the positive and odd, which are satisfied $p > q$ and $1 < p/q < 2$.

When $s = 0$, taking q/p powers on both sides of the equation

$$\eta_e^{q/p} + K^{q/p} \dot{\eta}_e = 0 \tag{30}$$

The control law can be designed as,

$$\tau = \tau_1 + \tau_2 \tag{31}$$
$$\tau_1 = C_{RB}\left(\upsilon\right) \upsilon - d_\upsilon - M_{RB}\left(J^{-1}\left(\eta\right)\left(\dot{J}\left(\eta\right) \upsilon_e + \hat{\dot{d}}_\eta + \frac{q}{p} K^{-1} diag\left(\dot{\eta}_e^{2-\frac{p}{q}}\right) - \dot{\upsilon}_R\right)\right) \tag{32}$$
$$\tau_2 = -\frac{\left(s^T K diag\left(\dot{\eta}_e^{\frac{p}{q}-1}\right) J\left(\eta\right) M_{RB}^{-1}\right)^T}{\left\| s^T K diag\left(\dot{\eta}_e^{\frac{p}{q}-1}\right) J\left(\eta\right) M_{RB}^{-1} \right\|^2} \left\| s \right\| \cdot \left\| s^T K diag\left(\dot{\eta}_e^{\frac{p}{q}-1}\right) J\left(\eta\right) M_{RB}^{-1} \right\| \Delta \tag{33}$$

$\Delta = diag\left(\Delta_1, \Delta_2, \Delta_3\right)$ are parameters to be set.

The stability of the system is demonstrated as following,

Theorem 1: The mathematical model (2) and finite-time disturbance observer of the USVs can ensure that all consistent signals and states are ultimately bounded under the control laws (31) and (32).

Proof: Firstly, the stability of the system is analyzed. For the system in (31), the sufficient conditions for the existence of terminal sliding mode are

$$\frac{1}{2} \frac{d}{dt} s^2 < -\delta \left| s \right| \tag{34}$$

where, $\delta > 0$. Combine the differencing of the sliding surface s with formula (29):

$$\dot{s} = \dot{\eta}_e + \frac{p}{q} K diag\left(\dot{\eta}_e^{\frac{q}{p}-1}\right)\left(\dot{J}\left(\eta\right) \upsilon_e + \times J\left(\eta\right)\left(\left(M_{RB}^{-1}\left(-C_{RB}\left(\upsilon\right) \upsilon + \tau_H + \tau\right)\right) + \tilde{\hat{d}}_\eta\right)\right. \tag{35}$$

According to the finite time error observer designed in the previous section, $\tilde{d}_\upsilon = \tau_H - \hat{d}_\upsilon$ is the disturbance estimation error. Meanwhile, there is an upper bound of disturbance

estimation error, and the upper bound is constant. In this way, the derivative of sliding surface s can be rewritten as follows,

$$\dot{s} = \frac{p}{q} K diag\left(\dot{\eta}_e^{\frac{q}{p}-1}\right)\left(J(\eta) M_{RB}^{-1}\left(\tilde{d}_v + \tau_2\right) + \tilde{\dot{d}}_\eta\right) \quad (36)$$

Both sides are multiplied by $\mathbf{s}^T$,

$$s^T \dot{s} = \frac{p}{q} K s^T diag\left(\dot{\eta}_e^{\frac{q}{p}-1}\right)\left(J(\eta) M_{RB}^{-1}\left(\tilde{d}_v + \tau_2\right) + \tilde{\dot{d}}_\eta\right) \quad (37)$$

Since p, q are positive and odd, and $p > q$, $1 < p/q < 2$. Then $0 < p/q - 1 < 1$. And $\eta_e \neq 0$, so $\eta_e^{p/q} > 0$. Therefore,

$$\dot{\delta} = \frac{p}{q} K \eta_e^{\frac{p}{q}-1}, \delta > 0 \quad (38)$$

When $\eta_e \neq 0$, there is

$$s^T \dot{s} \leq -\dot{\delta} |s| \quad (39)$$

Equation (39) shows that the controller satisfies the Lyapunov stability condition.

Next, it can be proved that the state can converge to zero in finite time t_s. Let t_s be the time from $s(0) \neq 0$ to $s = 0$. That is, when $t = t_s$, $s(t_s) = 0$. When $s > 0$, $t_s \leq -\frac{s(0)}{\delta}$. Meanwhile, when $s \leq 0$, $t_s \geq -\frac{s(0)}{\delta}$. So, $t_s \leq -\frac{|s(0)|}{\delta}$.

Given the time is t_r from $\eta_e \neq 0$ to $\eta_e = 0$, and at stage $s = 0$, then (40) can be rewritten as follows,

$$\eta_{ei}^{q/p} + k_i^{q/p} \dot{\eta}_{ei} = 0, (i = 1, 2, 3) \quad (40)$$

The above differential equation is transformed and integral:

$$\int_0^{t_r} dt = \int_{\eta_{ei}(0)}^{\eta_{ei}(t_r)} \left(-k_i^{q/p} \eta_{ei}^{-q/p}\right) d\eta_{ei} \quad (41)$$

According to the (41), it can be obtained that $t_{ri} = (k_i p/(p-q)) |\eta_{ei}(0)|^{(p-q)/p}$ can reach the equilibrium state along the sliding mode surface from any initial state that $\eta_{ei}(0) \neq 0$. Thus, it can be concluded that any point in the phase plane can be reached the sliding mode surface s = 0 in finite time. Hence, the nonsingular terminal sliding surface can be reached within finite time and the sliding mode state can reach zero in finite time. The proof is completed. □

IV. SIMULATION AND FIELD EXPERIMENT

In the simulation, it is assumed that there is a pool with 50 meters of length and width, in which there are two obstacles (represented by black circles) and a berth in the upper right corner, as shown in Fig. 6. The USV enters into the pool from the lower left corner to perform autonomous berthing. Given (35, 45) is the endpoint of the planned path, and (43, 45) is the endpoint after entering the berth. The starting point is (1, 1), the initial heading angle is $\psi_0 = \pi/6$, the maximum turning radius of the USV is 5m, the allowable error to the endpoint $\varepsilon = 1$m, and the maximum number of sampling points $N_m = 5000$. In order to ensure smooth entry into the berth, when arriving the endpoint of the path, 7 meters should be travelled along a straight line to fine tune the heading angle. The red point is the starting point, and the green point is the endpoint. Under the obstacle environment, our improved Dubins-RRT method is used to plan the berthing path. A total of 0.0975 seconds is taken, and the path planned is as shown in Fig. 6. The black path is the final obstacle-avoiding path, and the other colored paths are the abandoned paths. From Fig. 6, it can be seen that our improved Dubins-RRT algorithm can plan a relatively smooth path, which not only meets the obstacle avoidance requirements, but also satisfies the dynamics.

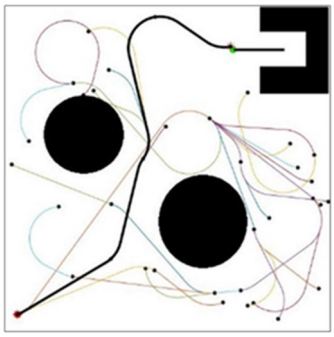

FIGURE 6. Obstacle avoidance path planned by Dubins-RRT.

In addition, to verify the validation of the proposed finite-time disturbance observer and non-singular terminal sliding mode controller, the path tracking experiment is carried out based on the USV designed by our laboratory. The USV experiment platform has a twin hulls, as shown in Fig. 7. It is with a mass of 21.2 kg, a length of 1.5 m, a width of 0.7 m, a moment of inertia $I_z = 20.24 kg \cdot m^2$ and a maximum power of 630 W for a single thruster [40]. Propulsion system is installed at the rear, and with no lateral propulsion. Sensors and positioning systems required for the experiment are also installed on the platform. The speed of the USV is 1m/s.

FIGURE 7. USV experimental platform and environment.

It can be seen that the path tracking and the designed path are relatively close in Fig.8. Due to the low accuracy of the positioning system and error accumulation caused by inertial navigation, it drifts in the second half path. The heading is shown in Fig. 9. Even subjecting to the delay and noise, there are some oscillations. But it can be also seen that the USV can follow the desired heading reference, the heading angle changes with the desired value, and the changing trend

is similar to the desired heading reference. The surge speed is illustrated in Fig. 10. It can be seen that the surge speed remains constant at about 1 m/s with oscillations. However, the surge speed response was able to reach the desired speed. It can be concluded that our controller design is effective.

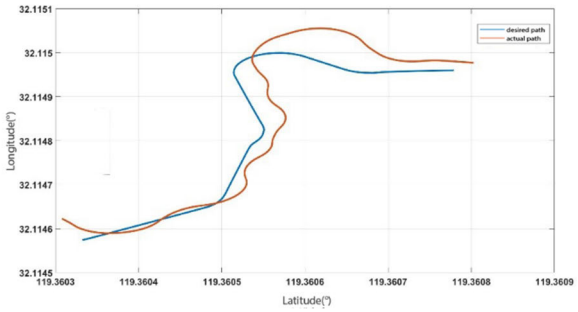

FIGURE 8. Results of Dubins-RRT path tracking experiment.

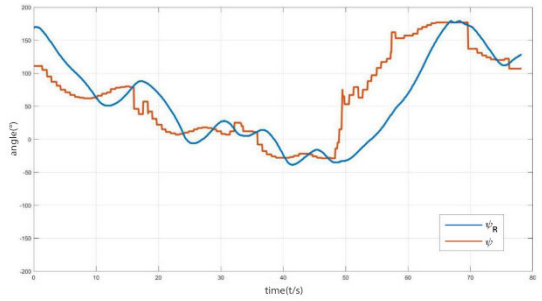

FIGURE 9. Yaw angle change of the USV.

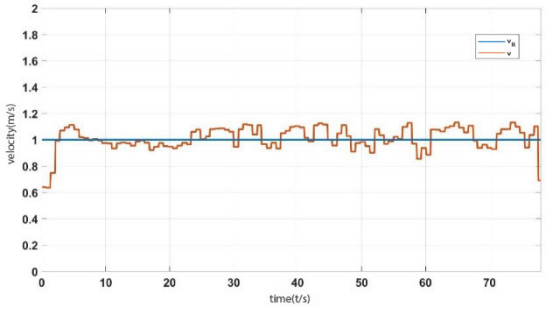

FIGURE 10. USV velocity change.

V. CONCLUSION

In the paper, the autonomous berthing of the USVs is divided into three parts: navigation, guidance, and control. To achieve obstacle avoidance and satisfy the underactuated dynamics of the USVs, a new improved Dubins-RRT algorithm is proposed to plan the path. The RRT algorithm is introduced to avoid obstacles, and the Dubins path is used to make the path smooth. In terms of path tracking controller design, firstly, the virtual target method is used to guide the USVs. Secondly, a corresponding finite-time disturbance observer is designed to estimate the uncertain terms in the USV model due to the lower speed and environmental disturbances. Finally, a non-singular sliding mode controller is devised to control the USVs, which can guarantee that the state variables reach stability within a finite time and achieve convergence of the tracking error. The feasibility of our algorithm is verified by simulation and experimentation.

REFERENCES

[1] N. Wang and H. Xu, "Dynamics-constrained global-local hybrid path planning of an autonomous surface vehicle," *IEEE Trans. Veh. Technol.*, vol. 69, no. 7, pp. 6928–6942, Jul. 2020, doi: 10.1109/TVT.2020.2991220.

[2] H. R. Karimi and Y. Lu, "Guidance and control methodologies for marine vehicles: A survey," *Control Eng. Pract.*, vol. 111, Jun. 2021, Art. no. 104785.

[3] N. Wang and H. R. Karimi, "Successive waypoints tracking of an underactuated surface vehicle," *IEEE Trans. Ind. Informat.*, vol. 16, no. 2, pp. 898–908, Feb. 2020, doi: 10.1109/TII.2019.2922823.

[4] H. Mousazadeh, H. Jafarbiglu, H. Abdolmaleki, E. Omrani, F. Monhaseri, M.-R. Abdollahzadeh, A. Mohammadi-Aghdam, A. Kiapei, Y. Salmani-Zakaria, and A. Makhsoos, "Developing a navigation, guidance and obstacle avoidance algorithm for an unmanned surface vehicle (USV) by algorithms fusion," *Ocean Eng.*, vol. 159, no. 6, pp. 56–65, Jul. 2018.

[5] S. Baek and J. Woo, "Model reference adaptive control-based autonomous berthing of an unmanned surface vehicle under environmental disturbance," *Machines*, vol. 10, no. 4, p. 244, Mar. 2022, doi: 10.3390/MACHINES10040244.

[6] Y. Zhang, M. Y. Zhang, and Q. Zhang, "Auto-berthing control of marine surface vehicle based on concise backstepping," *IEEE Access*, vol. 8, pp. 197059–197067, 2020, doi: 10.1109/ACCESS.2020.3034491.

[7] Y. Liao, Z. Jia, W. Zhang, Q. Jia, and Y. Li, "Layered berthing method and experiment of unmanned surface vehicle based on multiple constraints analysis," *Appl. Ocean Res.*, vol. 86, pp. 47–60, May 2019.

[8] Z. He, C. Liu, X. Chu, R. R. Negenborn, and Q. Wu, "Dynamic anti-collision A-star algorithm for multi-ship encounter situations," *Appl. Ocean Res.*, vol. 118, Jan. 2022, Art. no. 102995.

[9] W. Liu, K. Qiu, X. Yang, R. Wang, Z. Xiang, Y. Wang, and W. Xu, "COLREGS-based collision avoidance algorithm for unmanned surface vehicles using modified artificial potential fields," *Phys. Commun.*, vol. 57, Apr. 2023, Art. no. 101980.

[10] J. Wang, W. Chi, C. Li, C. Wang, and M. Q.-H. Meng, "Neural RRT: Learning-based optimal path planning," *IEEE Trans. Autom. Sci. Eng.*, vol. 17, no. 4, pp. 1748–1758, Oct. 2020, doi: 10.1109/TASE.2020.2976560.

[11] B. Liu, W. Feng, T. Li, C. Hu, and J. Zhang, "A variable-step RRT path planning algorithm for quadrotors in below-canopy," *IEEE Access*, vol. 8, pp. 62980–62989, 2020.

[12] I. B. Jeong, S. J. Lee, and J. H. Kim, "Quick-RRT: Triangular inequality-based implementation of RRT with improved initial solution and convergence rate," *Expert Syst. Appl.* vol. 123, pp. 82–90, Jun. 2019.

[13] Y. Li, W. Wei, Y. Gao, D. Wang, and Z. Fan, "PQ-RRT: An improved path planning algorithm for mobile robots," *Expert Syst. Appl.*, vol. 152, Aug. 2020, Art. no. 113425.

[14] C. Chen, X.-Q. Chen, F. Ma, X.-J. Zeng, and J. Wang, "A knowledge-free path planning approach for smart ships based on reinforcement learning," *Ocean Eng.*, vol. 189, Oct. 2019, Art. no. 106299.

[15] S. Guo, X. Zhang, Y. Zheng, and Y. Du, "An autonomous path planning model for unmanned ships based on deep reinforcement learning," *Sensors*, vol. 20, no. 2, p. 426, Jan. 2020.

[16] S. Guo, X. Zhang, Y. Du, Y. Zheng, and Z. Cao, "Path planning of coastal ships based on optimized DQN reward function," *J. Mar. Sci. Eng.*, vol. 9, no. 2, p. 210, Feb. 2021.

[17] Y. Xiaofei, S. Yilun, L. Wei, Y. Hui, Z. Weibo, and X. Zhengrong, "Global path planning algorithm based on double DQN for multi-tasks amphibious unmanned surface vehicle," *Ocean Eng.*, vol. 266, Dec. 2022, Art. no. 112809.

[18] N. Gu, D. Wang, Z. Peng, J. Wang, and Q.-L. Han, "Advances in line-of-sight guidance for path following of autonomous marine vehicles: An overview," *IEEE Trans. Syst., Man, Cybern., Syst.*, vol. 53, no. 1, pp. 12–28, Jan. 2023, doi: 10.1109/TSMC.2022.3162862.

[19] Z. Yan, H. Yu, W. Zhang, B. Li, and J. Zhou, "Globally finite-time stable tracking control of underactuated UUVs," *Ocean Eng.*, vol. 107, pp. 132–146, Oct. 2015.
[20] L. Liu, D. Wang, Z. Peng, and H. Wang, "Predictor-based LOS guidance law for path following of underactuated marine surface vehicles with sideslip compensation," *Ocean Eng.*, vol. 124, pp. 340–348, Sep. 2016.
[21] A. M. Lekkas and T. I. Fossen, "Integral LOS path following for curved paths based on a monotone cubic Hermite spline parametrization," *IEEE Trans. Control Syst. Technol.*, vol. 22, no. 6, pp. 2287–2301, Nov. 2014.
[22] T. I. Fossen and A. M. Lekkas, "Direct and indirect adaptive integral line-of-sight path-following controllers for marine craft exposed to ocean currents," *Int. J. Adapt. Control Signal Process.*, vol. 31, no. 4, pp. 445–463, Apr. 2017.
[23] Z. Cai, L. Wang, J. Zhao, K. Wu, and Y. Wang, "Virtual target guidance-based distributed model predictive control for formation control of multiple UAVs," *Chin. J. Aeronaut.*, vol. 33, no. 3, pp. 1037–1056, Mar. 2020.
[24] Z. Chen and S. S. Ge, "Cascaded design for robust trajectory tracking control of an underactuated surface vehicle," in *Proc. China Autom. Congr. (CAC)*, Beijing, China, Oct. 2021, pp. 7565–7570.
[25] Y. Zhao, X. Sun, G. Wang, and Y. Fan, "Adaptive backstepping sliding mode tracking control for underactuated unmanned surface vehicle with disturbances and input saturation," *IEEE Access*, vol. 9, pp. 1304–1312, 2021, doi: 10.1109/ACCESS.2020.3046130.
[26] B. Du, B. Lin, C. Zhang, B. Dong, and W. Zhang, "Safe deep reinforcement learning-based adaptive control for USV interception mission," *Ocean Eng.*, vol. 246, Feb. 2022, Art. no. 110477.
[27] D. Wang and M. Fu, "Adaptive formation control for waterjet USV with input and output constraints based on bioinspired neurodynamics," *IEEE Access*, vol. 7, pp. 165852–165861, 2019, doi: 10.1109/ACCESS.2019.2953563.
[28] S. Ding, B. Zhang, K. Mei, and J. H. Park, "Adaptive fuzzy SOSM controller design with output constraints," *IEEE Trans. Fuzzy Syst.*, vol. 30, no. 7, pp. 2300–2311, Jul. 2022.
[29] L. Ma, K. Mei, S. Ding, and T. Pan, "Design of adaptive fuzzy fixed-time HOSM controller subject to asymmetric output constraints," *IEEE Trans. Fuzzy Syst.*, early access, Jan. 31, 2023, doi: 10.1109/TFUZZ.2023.3241147.
[30] A. Gonzalez-Garcia and H. Castaneda, "Guidance and control based on adaptive sliding mode strategy for a USV subject to uncertainties," *IEEE J. Ocean. Eng.*, vol. 46, no. 4, pp. 1144–1154, Oct. 2021, doi: 10.1109/JOE.2021.3059210.
[31] N. Wang and C. Ki Ahn, "Hyperbolic-tangent LOS guidance-based finite-time path following of underactuated marine vehicles," *IEEE Trans. Ind. Electron.*, vol. 67, no. 10, pp. 8566–8575, Oct. 2020.
[32] N. Wang, H. R. Karimi, H. Li, and S.-F. Su, "Accurate trajectory tracking of disturbed surface vehicles: A finite-time control approach," *IEEE/ASME Trans. Mechatronics*, vol. 24, no. 3, pp. 1064–1074, Jun. 2019.
[33] W. Liu, H. Ye, and X. Yang, "Super-twisting sliding mode control for the trajectory tracking of underactuated USVs with disturbances," *J. Mar. Sci. Eng.*, vol. 11, no. 3, p. 636, Mar. 2023.
[34] H. Huang and Y. Fan, "Sliding mode based ADRC for curved path following of unmanned surface vessels," in *Proc. Chin. Autom. Congr. (CAC)*, Jinan, China, Oct. 2017, pp. 4198–4202, doi: 10.1109/CAC.2017.8243516.
[35] M. Li, C. Guo, Y. Yuan, and M. Guo, "Path following control of the asymmetric USV via backsteppin sliding mode technique," in *Proc. Chin. Control Decis. Conf. (CCDC)*, Nanchang, China, Jun. 2019, pp. 2979–2984, doi: 10.1109/CCDC.2019.8833109.
[36] Y. Yu, C. Guo, and H. Yu, "Finite-time PLOS-based integral sliding-mode adaptive neural path following for unmanned surface vessels with unknown dynamics and disturbances," *IEEE Trans. Autom. Sci. Eng.*, vol. 16, no. 4, pp. 1500–1511, Oct. 2019, doi: 10.1109/TASE.2019.2925657.
[37] T. I. Fossen, "Handbook of marine craft hydrodynamics and motion control," in *Handbook of Marine Craft Hydrodynamics and Motion Control*. Hoboken, NJ, USA: Wiley, 2011, doi: 10.1002/9781119994138.
[38] J. N. Wilburn, M. G. Perhinschi, and B. K. Wilburn, "Implementation of a 3-dimensional dubins-based UAV path generation algorithm," in *Proc. AIAA Guid., Navigat., Control (GNC) Conf.*, Aug. 2013, pp. 1–10.
[39] Y. B. Shtessel, I. A. Shkolnikov, and A. Levant, "Smooth second-order sliding modes: Missile guidance application," *Automatica*, vol. 43, no. 8, pp. 1470–1476, Aug. 2007.
[40] X. Yang, X. Yan, W. Liu, H. Ye, Z. Du, and W. Zhong, "An improved Stanley guidance law for large curvature path following of unmanned surface vehicle," *Ocean Eng.*, vol. 266, Dec. 2022, Art. no. 112797.

FEIFEI SONG was born in Henan, China, in 1986. She received the B.E. degree in automation from the Zhengzhou University of Light Industry, in 2009, and the M.S. degree in systems engineering from the Nanjing University of Aeronautics and Astronautics, in 2013. Currently, she is teaching with the Department of Medical Information Engineering, Kangda College of Nanjing Medical University. Her research interests include artificial intelligence application, USV control, and image processing.

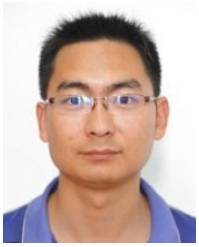

XIAOFEI YANG (Member, IEEE) was born in Henan, China, in 1983. He received the B.E. degree in electronical information science and technology from the Nanjing University of Technology, China, in 2005, and the M.S. degree in circuits and systems and the Ph.D. degree in automatic control from the Nanjing University of Science and Technology, China, in 2007 and 2011, respectively. He is currently an Associate Professor with the School of Electronics and Information, Jiangsu University of Science and Technology. His research interests include control theory for autonomous systems, the IoT, and RF systems.

ZHENGRONG XIANG (Member, IEEE) received the Ph.D. degree in control theory and control engineering from the Nanjing University of Science and Technology, Nanjing, China, in 1998. He was a Lecturer and an Associate Professor with the Nanjing University of Science and Technology, in 1998 and 2001, respectively, where he is currently a Full Professor. His research interests include switched systems, nonlinear control, robust control, and networked control systems. He is a member of the Chinese Association for Artificial Intelligence.